Eur. Phys. J. B **45**, 433–442 (2005)
DOI: 10.1140/epjb/e2005-00201-9

THE EUROPEAN PHYSICAL JOURNAL B

Formation of ripples over a sand bed submitted to a turbulent shear flow

A. Valance[a]

Groupe Matière Condensée et Matériaux, CNRS UMR 6626, Université Rennes 1, 35042 Rennes Cedex, France

Received 16 February 2005
Published online 6 July 2005 –

Abstract. We investigate the process of ripple formation when a sand bed is submitted to a steady and turbulent liquid flow. The sand transport dynamics is described in terms of a simple relaxation law which accounts for the fact that the transport rate does not adapt instantaneously to its equilibrium value. The equilibrium sand flux is evaluated using a standard law based on the estimation of the flow shear stress calculated at the sand bed surface. The latter is estimated from an analytical resolution of the flow over a deformed sand bed which is based on the Jackson and Hunt calculation [J.C.R. Hunt, Quart. J. R. Met. Soc. **101**, 929 (1975)]. Within this model, we investigate the stability of the sand bed and are able to derive analytical scaling laws for the wavelength and phase velocity of the most dangerous mode. In the deep flow limit, the model predicts the occurrence of a single mode of instability corresponding to the formation of ripples. Predictions of our model are compared with previous models and available experimental data.

PACS. 45.70.-n Granular systems – 47.27.-i Turbulent flows, convection, and heat transfer – 47.54.+r Pattern selection; pattern formation

1 Introduction

Ripples on sand are observed in seas (or rivers) but also in deserts. One important issue is to identify the underlying physical mechanisms responsible for the development of sand ripples. Despite the abundant literature on the subject, the pertinent mechanisms have not been yet clearly identified. Indeed, while it is largely admitted that the destabilizing mechanism of a flat sand bed is due to the fluid flow, the stabilizing one is still matter of debate. The latter is very important because it balances the fluid flow destabilizing effect and leads to the selection of a fastest growing mode, which is expected to give an order of magnitude of the ripple wavelength in the first stages of its development. We propose here a new model for steady and turbulent liquid flows in which we introduce a new stabilizing mechanism resulting from the inertia of the grains. We should emphasize that we deal with steady flows and not with oscillatory flows, which constitute an other class of flows.

First of all, we find it worthwhile to recall the basic mechanisms of sand transport in a liquid and the strategies used in the literature to describe the sand ripple formation process. In a liquid, there exists two main modes of sediment transport, the bed load and the suspended load [1]. The latter is usually neglected in most models since it becomes significative only at high flow rate. The bed load is the part of the load that is in continuous contact during the transport; it corresponds to the grains that are rolling over the sand bed surface. The transport rate corresponding to the bed load is determined almost exclusively by the fluid shear stress acting directly on the sand bed. The strategy to investigate the ripple formation is therefore to calculate the flow shear stress over the sand bed and to deduce the sediment transport rate. Then, the evolution of the bed profile is derived from mass conservation law. In addition, it is usually assumed that the hydrodynamical time is much small than the morphological one. Therefore the essential difficulty is to calculate the turbulent fluid flow over a deformed surface.

The first theoretical approaches were based on potential flow models [2–5] but they were not able to predict the existence of sand ripple instability. The first theoretical models calculating explicitly the turbulent flow profile over a deformed sand bed are due to Richards and to Sumer et al. in the eighties [6,7]. In the Richards model the turbulent flow is modeled via an eddy-viscosity approach based on an additional equation for the turbulent kinetic energy. The outcomes of his model are the following. (i) The destabilizing mechanism for the bed instability originates from hydrodynamics. The bed shear stress, as in a laminar shear flow, is not in phase with the bed profile, which generates the bed instability. (ii) The stabilizing mechanism is found to originate from gravitational force which impedes grain motion up stoss slopes and aids it down lee slope. (iii) The competition between

[a] e-mail: alexandre.valance@univ-rennes1.fr

these two mechanisms leads to the existence of a band of unstable modes corresponding to small scale structures (that is ripples). It is found that the wavelength of the ripple mode scales as $\lambda \sim f(\phi_s)y_0$, where f is an increasing function of ϕ_s characterizing the intern angle of friction of the granular material, and y_0 is the roughness height of the bed. The estimation of the roughness height is difficult since it depends on intricate parameters such as the flow shear stress, the height of the bed-load layer and the grain diameter. As a first approximation, it scales with the grain diameter and the value adopted generally on erodible bed is $y_0 \simeq 2\,d - 4\,d$ [8]. Taking this value, the prediction of the model gives a ripple wavelength compatible with the experimental observations [9]. Sumer and Bakioglu [7] extended the Richards model to include the viscosity effect which is expected to be effective when the viscous sublayer is greater than the grain diameter (i.e., when the particle Reynolds number is smaller than 25 [7]). In such a regime, the ripple wavelength is found to scale as $\lambda \simeq (\nu/U^*)\, f(dU^*/\nu)$, where ν is the fluid viscosity, U^* is the shear velocity, and f is a weakly increasing function of the particle Reynolds number. In contrast with Richards results, the ripple wavelength appears therefore not to scale with the grain size d.

At last, one should mention that arguments based on the turbulent bursting process have been proposed to explain the ripple instability [10]. However, one can argue that the ripple instability also occurs in laminar flows and that therefore turbulence is not necessarily the pertinent mechanism of instability [11].

None of these models take into account the effect of the grain inertia which is expected to be effective at large particle Reynolds number. The model we propose is inspired from that presented in [12] for laminar flows and is applied to the case of turbulent flows. More precisely, we introduce an additional stabilizing mechanism resulting from the effect of grain inertia. The bed shear stress over a deformed bed is derived analytically on the basis of the calculation of Jackson and Hunt [13], which allows to derive analytical scaling laws for the most unstable mode. The analysis presented here is restricted to the case where the sand bed is hydraulically rough, namely, for high enough particle Reynolds number ($Re_p^* > 25$).

The article is organized as follows. In Section 2, we present the model equations for the turbulent flow and the sediment transport. The basic solution of the model corresponding to a flat sand bed is briefly analyzed in Section 3. Section 4 is devoted to the presentation of the linear stability analysis of the flat sand bed. The predictions of the model (i.e., growth rate and drift velocity of unstable modes) are analyzed. Finally, discussion and conclusion are presented in Section 5.

2 Model equations

We consider a turbulent boundary layer that has developed over a planar rough wall of constant roughness. Provided that the horizontal scale of the bed deformation is much less than the distance required for the boundary layer to change appreciably, the width L of the boundary layer may be taken as independent of the downstream distance. Above the boundary layer, the flow is assumed to be uniform ($U = U_\infty = Cst$). Furthermore, we will restrict ourselves to a two-dimensional analysis. In other words, we assume that the bed deformation is invariant along the horizontal direction perpendicular to the flow. We first briefly present the equations for turbulent flows together with the boundary conditions employed. Then we describe the model used for sediment transport.

2.1 Turbulent flow equations

We use the hypothesis of quasi-stationarity. The flow is considered to be stationary with respect to the typical time of morphological bed deformation. This means that the equations of the flow should be solved in the stationary regime where the bed profile is static. At last, it should be noted that the velocity profile over the sand bed is determined for a flow free of sediment. The rate of sediment transport is then estimated as a function of the bed shear stress calculated for such a flow free of sediment. In other words, we do not calculate the actual velocity flow profile which results from the non-trivial coupling between the flow and the transported grains. The explicit treatment of this coupling would require a much more sophisticated model.

The governing equations for a fully developed turbulent flow are:

$$\rho_f(\boldsymbol{u}\cdot\boldsymbol{\nabla})\boldsymbol{u} = -\boldsymbol{\nabla}p + \eta\nabla^2\boldsymbol{u} + \boldsymbol{\nabla}\cdot\bar{\bar{\tau}}\,, \tag{1}$$

$$\boldsymbol{\nabla}\cdot\boldsymbol{u} = 0\,. \tag{2}$$

$\boldsymbol{u} = (U, V)$ is the mean flow velocity, p the mean pressure, and $\bar{\bar{\tau}}$ is the Reynolds stress tensor which reads:

$$\tau_{xx} = 2\rho_f\nu_t^h\,(\partial_x U)\,,\quad \tau_{yy} = 2\rho_f\nu_t\partial_y V\,, \tag{3}$$

$$\tau_{xy} = \tau_{yx} = \rho_f[\nu_t\,(\partial_y U) + \nu_t^h\,(\partial_x V)]\,. \tag{4}$$

ν_t and ν_t^h are respectively the vertical and horizontal turbulent eddy viscosity. It turns out that the terms containing ν_t^h do not play a significant role in the analysis, and only the vertical viscosity is important. Using the mixing length theory [14], the vertical turbulent viscosity is given by:

$$\nu_t = l^2(\partial_y U)\,, \tag{5}$$

where l is the mixing length. Prandtl [14] assumed that l increases linearly with the distance Y from the bed surface: $l = \kappa Y$, where κ is the von Karman constant ($\kappa \approx 0.4$) and $Y = y - h(x)$ [$h(x)$ measuring the height of the bed profile].

The boundary conditions at the distance L from the bottom of the flow are:

$$U = U_\infty \text{ and } V = 0\,, \tag{6}$$

while at the sand bed, we use zero slip conditions:

$$U = V = 0\,, \tag{7}$$

taken at $y = h(x) + y_0$, where y_0 is the effective roughness of the sand bed.

We find it worthwhile to calculate, at this point, the velocity profile of a turbulent boundary layer over a flat surface in order to introduce the notion of shear velocity that will be needed later on. In the case of a flow over a flat surface, neglecting the viscous term the equation (1) reduces to:

$$\frac{\partial}{\partial y}\tau_{xy} = 0\,, \tag{8}$$

where the shear stress τ_{xy} is given by:

$$\tau_{xy} = \rho_f \kappa^2 y^2 \left(\frac{\partial U}{\partial y}\right)^2 . \tag{9}$$

τ_{xy} is constant (i.e., independent of the height y) and equal to the shear force σ per unit area exerted on the bed (termed also the bed shear stress). We usually introduce the shear velocity U^* defined as $U^* = \sqrt{\sigma/\rho_f}$. We can rewrite equation (9) as:

$$\frac{\partial U}{\partial y} = \frac{U^*}{\kappa y}\,. \tag{10}$$

Integrating this equation, we obtain the well-know logarithmic profile for a turbulent flow near a rough wall:

$$U(y) = \frac{U^*}{\kappa}\ln\left(\frac{y}{y_0}\right)\,, \tag{11}$$

where we recall that y_0 is the bed roughness. For a fixed bed made of single grain size d, it is found that $y_0 = d/30$ in the case of hydraulically rough beds [15]. However, for erodible bed, this value is increased: $y_0 \approx 2d - 4d$ [8].

At this point, we shall point out that we will restrict our analysis to hydraulically rough beds. This means that we neglect the presence of the viscous sublayer which is much smaller than the grain size in hydraulically rough regimes.

2.2 Sediment transport

The volumetric transport law q is linked to the height h of the bed profile via the mass conservation equation

$$\frac{\partial h}{\partial t} = -\frac{\partial q}{\partial x}\,. \tag{12}$$

In standard models, the sand flux is usually taken to be equal to an 'equilibrium' value q_{eq} estimated from a steady and fully developed situation. The equilibrium sand flux is generally evaluated using semi-empirical laws based on the estimation of the bed shear stress [1]:

$$q_{eq} = q_b\left(\Theta - \Theta_{c0}\left(1 + \frac{h_x}{\tan\phi_s}\right)\right)^n\,, \tag{13}$$

with $q_b = c\sqrt{(s-1)\rho_f g d^3}$. The parameter ϕ_s is the friction angle of the sand, and $\Theta = \sigma/(\rho_f(s-1)gd)$ is the Shield number of the flow (σ being the local flow shear stress at the bed and $s = \rho_g/\rho_f$ the relative density of the sediment with respect to the fluid density). Θ_{c0} indicates the critical Shields number above which sediments start to move over a flat bed. For practical purpose, we will take $\Theta_{c0} = 0.2$. Finally, the exponent n of the transport rate varies from one author to one another. In the Peter-Meyer law [1], $n = 3/2$. Note however that the value of the exponent is unimportant for a linear stability analysis.

The equilibrium sand flux corresponds to the maximum transport rate that a flow can sustain in an equilibrium situation (i.e., steady and fully developed) for a given shear stress. In standard models, it is therefore implicitly assumed that the transport rate is everywhere equal to this equilibrium flux. However, in out-of-equilibrium situations, one can expect that the transport rate does not instantaneously adapt to its equilibrium value. Indeed, if the fluid velocity increases, new grains (initially at rest) are dragged by the flow and they need some time to reach their equilibrium velocity (due to their inertia). This characteristic time can be associated with an equilibrium length l_{eq} corresponding to the distance needed for the grains, initially at rest, to equilibrate their velocity with that of the fluid. This concept of equilibrium length has been first introduced in the context of aeolian sand transport [16,17] and later applied in the case of sediment transport in a liquid [12]. To describe the dynamics of sand transport, we will use a simple relaxation law of the form:

$$\frac{\partial q}{\partial x} = -\frac{q - q_{eq}}{l_{eq}}\,. \tag{14}$$

It remains to evaluate the equilibrium length using physical arguments. As already mentioned in [12], the precise determination of l_{eq} is not a simple task due to the complex feedback interaction between the moving grains and the fluid. As a first approach, we will make a simplified calculation following the same lines as those exposed in [12]. We will assume that the moving grains roll on the sand surface and undergo a drag force, $F_d = 0.125\, c_d\, \rho_f \pi d^2\, v_r^2$, where v_r is the relative velocity of the grains with respect to that of the fluid and c_d is the drag coefficient. The coefficient c_d will be taken to be equal to $c_d = 24./Re + 6./(1+\sqrt{Re}) + 0.4$ with $Re = dv_r/\nu$. Within these approximations, one obtains:

$$l_{eq} = f(dU_{eq}/\nu)\frac{\rho_f}{\rho_g}d\,, \tag{15}$$

where U_{eq} is the equilibrium velocity of the grains and f is a function of the dimensionless number dU_{eq}/ν. In the case of hydraulically rough beds, the order of magnitude of U_{eq} is expected to be given by the shear velocity $U^* = \sqrt{\sigma/\rho_f}$. Therefore, we will set $U_{eq} = \xi U^*$ where ξ is a numerical constant of order of few units. We will also introduce the turbulent particle Reynolds number Re_p^* defined as $Re_p^* = dU^*/\nu$. The variation of l_{eq} with the particle Reynolds number is shown in Figure 1. When $Re_p^* < 1$, $f \approx 0.035\,\xi Re_p^*$, and for $Re_p^* > 10^4$, f reaches a constant equal to 3.3. For intermediate particle Reynolds

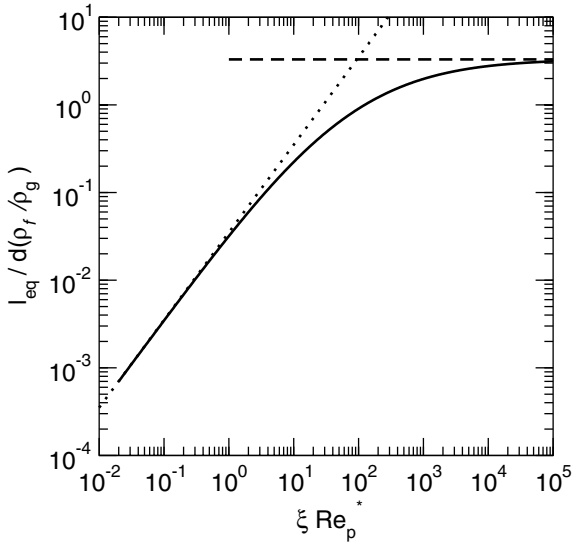

Fig. 1. Equilibrium length versus ξRe_p^*. Re_p^* is the turbulent particle Reynolds number: $Re_p^* = d\,U^*/\nu$. For $Re_p^* < 10$, $l_{eq} \sim Re_p^*\,d$ (dotted curve), whereas l_{eq} becomes independent of Re_p^* for large Re_p^* (dashed curve).

number (i.e., $1 < Re_p^* < 10^3$), f can be approximated by: $f(\xi Re_p) \approx 0.035\,\xi Re_p/[1 + 0.087(\xi Re_p)^{0.75}]$.

3 Basic state

The basic state corresponds to the solution of the problem equations for which the sand bed remains flat. In that case, we have already see that the velocity profile reads:

$$U_0(y) = \frac{U^*}{\kappa} \ln\left(\frac{y}{y_0}\right) \tag{16}$$

with $U^* = \sqrt{\sigma_0/\rho_f}$ (where σ_0 is the bed shear stress). The total flux of sediment transport therefore reads:

$$q_0 = c\frac{\sqrt{(s-1)\rho_f\, g\, d^3}}{((s-1)gd)^n}\left(\frac{U^{*2}}{(s-1)gd} - \frac{U_c^{*2}}{(s-1)gd}\right)^n , \tag{17}$$

where U_c^* is the critical shear velocity above which sediment starts to move: $U_c^{*2} = (s-1)gd\Theta_{c0}$. We recall that c is a numerical constant. For $n = 3/2$, the sediment transport rate takes the following simple form:

$$q_0 = c\frac{\rho_f}{(s-1)g}\left(U^{*2} - U_c^{*2}\right)^{3/2} . \tag{18}$$

4 Linear stability analysis

In order to study the stability of the flat sand bed, we perturb the sand bed profile so that it looks like $h = h_1 e^{ikx+\omega t}$, where k is the wavenumber characterizing the spacing of the crests and ω denotes the growth rate of the bed pattern.

4.1 Perturbed flow

We first calculate the flow perturbation, the bed profile being kept fixed. The calculation strategy used here is inspired from that developed by Jackson and Hunt [13] and improved later by Hunt, Leibovich and Richards, and Weng and his collaborators [18,19]. This is a lengthy and tough calculation, that we present in Appendix A in a reassessed version accessible to non-specialists of turbulent flows. One should also add that we treat the situation where the sand bed perturbation is spatially periodic whereas the former analyses investigated the case of a spatially isolated perturbation of the bed.

It is found that the bed shear stress over a deformed sand bed is given by:

$$\sigma = \sigma_0 + \sigma_1 = \sigma_0 + \hat{\sigma}_1 e^{ikx} , \tag{19}$$

where

$$\hat{\sigma}_1 = 2A\,h_1|k|[1 + \delta(1 + 4\gamma + i\pi)] . \tag{20}$$

$\delta \simeq 0.65(ky_0)^{0.15}$, $\delta_1 = \ln^{-1}(1/ky_0)$, γ is the Euler constant ($\gamma = 0.57$) and $A = \delta^2/\delta_1^2$ (see Appendix A for more details).

4.2 Growth rate and drift velocity

We are now in position to calculate the growth rate ω of the perturbation. Linearizing equations (12) and (14) together with equation (13), we get:

$$\omega = n\,q_b\,\Theta_{c0}^n\;\mu^{n-1}\left[-i\frac{\Theta_1}{\Theta_{c0}}\frac{k}{h_1} - \frac{k^2}{\tan\phi_s}\right]\frac{(1 - ikl_{eq})}{(1 + k^2 l_{eq}^2)} , \tag{21}$$

where $\mu = (\Theta_0 - \Theta_{c0})/\Theta_{c0}$ (or equivalently $\mu = U^{*2}/U_c^{*2} - 1$) and $\Theta_1 = \hat{\sigma}_1/(s-1)\rho_f g\,d$. μ measures the distance from the threshold of grain motion and will be referred to as the relative shear stress excess.

The dispersion relation expanded in the long wavelength limit yields:

$$\mathrm{Re}(\omega) = \omega_0\,\mu^{n-1}\left[2\,\pi\,A\,\delta\,(1+\mu)\,k|k|\,d^2 - \frac{k^2\,d^2}{\tan\phi_s} - 2\,A\,(1+\mu)k^2|k|\,l_{eq}d^2\right] , \tag{22}$$

$$\mathrm{Im}(\omega) = -2\,\omega_0\,A\,\mu^{n-1}(1+\mu)\,k|k|d^2 . \tag{23}$$

We set $\omega_0 = n(q_b/d^2)\Theta_{c0}^n$. The real part of the growth rate is composed of three terms. The first one plays a destabilizing role and is due to the fluid flow. The two next terms are stabilizing ones, one is due to gravity and the other to grain inertia. One can note that the fluid flow effect and the gravity effect both scale as k^2. This means that if the latter prevails, all modes are stable and the bed surface is stable. On the contrary, in the case that the destabilizing effect of the fluid flow is predominant, one expects the existence of a band of unstable modes. Let us estimate the magnitude of these two contradictory mechanisms and determine the critical shear stress excess,

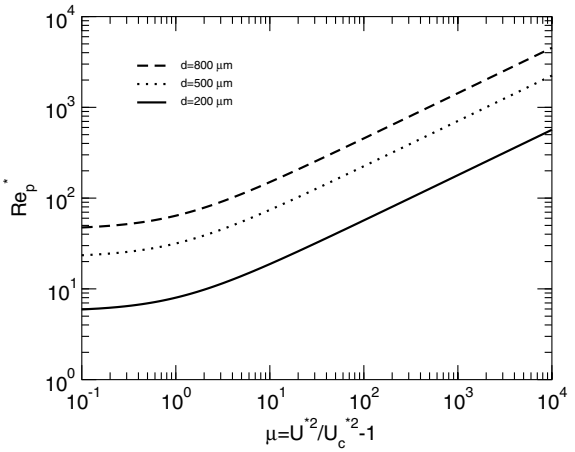

Fig. 2. Correspondence between the particle Reynolds number and the relative shear stress excess μ. $\theta_{0c} = 0.2$, $s = 2.7$, $\xi = 5$ and $\nu = 10^{-6}\,\mathrm{m}^2/\mathrm{s}$.

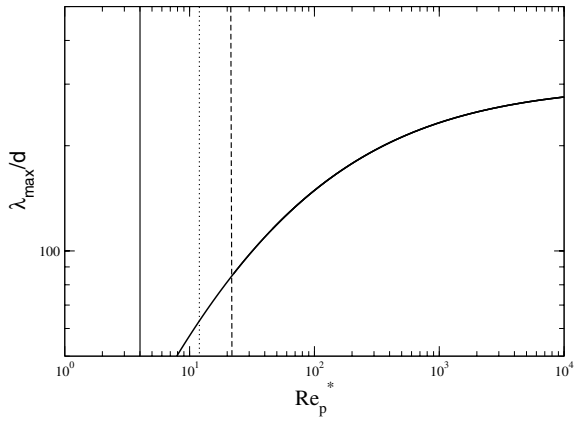

Fig. 3. Wavelength of the most dangerous mode versus the particle Reynolds number. The vertical lines indicate the values of the critical particle Reynolds number (corresponding to the onset of grain motion) respectively for $d = 200, 500, 800\,\mu$m. Parameters: $\theta_{0c} = 0.2$, $s = 2.7$, $\xi = 5$ and $\nu = 10^{-6}\,\mathrm{m}^2/\mathrm{s}$.

μ_c, for which both effects have the same magnitude. One obtains:

$$\mu_c = (2\,A\,\delta\,\pi\tan\phi_s)^{-1} - 1\,. \tag{24}$$

When $\mu < \mu_c$, the gravity effect prevails and the flat bed is stable. An estimation of the parameters A and δ gives: $A = 2$ and $\delta = 0.4$. We took standard values for the roughness y_0 and the wavenumber k ($y_0 \approx d$ and $1/k \approx 200\,d$). Note however that an accurate evaluation of y_0 and k is not necessary here since the parameters A and δ_1 depend only weakly on them (see previous section). Using these values and taking a standard value for the intern angle of friction ($\phi_s = 30°$), we get $\mu_c \approx -0.86$. A negative value of μ means that the bed shear stress is below the critical shear stress corresponding to the onset of grain motion. As a consequence, one can conclude that as soon as grain motion is possible (i.e., $\mu > 0$), the stabilizing gravity effect is unable to overcome the destabilizing effect of the fluid flow. In other words, the sand bed is always unstable when the sand transport is possible. Gravity effect plays a minor role and it is therefore legitimate to neglect it.

At higher wave numbers, the destabilizing effect of the fluid flow will be balanced by the stabilizing effect of grain inertia (that scales as k^3) leading to the selection of a fastest growing mode. Neglecting the gravity effect, the fastest growing mode can be easily estimated:

$$k_{max}\,l_{eq} = \frac{2\,\pi\delta}{3}\,, \tag{25}$$

or equivalently

$$\lambda_{max} = \frac{2\pi}{k_{max}} = \frac{3}{\delta} l_{eq}\,. \tag{26}$$

We recall that $l_{eq} = f(\xi Re_p^*)\,(\rho_f/\rho_g)d$ where $Re_p^* = U^*\,d/\nu$ is the turbulent particle Reynolds number whose variation with the relative shear stress excess μ is shown in Figure 2. As mentioned previously, our analysis is expected to be valid in the hydraulically rough regime, namely, when the particle Reynolds number is greater than 25. Sand beds constituted of coarse grains ($d > 500\,\mu$m) are hydraulically rough at the onset of grain motion and above. In the case of finer grains, the sand bed becomes hydraulically rough only at large shear stress excess (see Fig. 2).

The evolution of the wavelength of the most dangerous mode as a function of the particle Reynolds number is shown in Figure 3. One can note that λ_{max} increases with the particle Reynolds number and reaches an asymptotic value at large Re_p^*. In the latter regime ($Re_p^* > 10^4$), the equilibrium length becomes independent of the shear velocity U^* [$l_{eq} \approx 3.3(\rho_g/\rho_f)d$] and one obtains the following scaling for λ_{max}:

$$\lambda_{max} = 100.\,\frac{\rho_g}{\rho_f}\,d\,. \tag{27}$$

In the above estimation, we took $\delta = 0.4$. In water for grains of diameter $d = 200\,\mu m$, we obtain $\lambda_{max} \approx 6\,cm$.

It can be interesting to replot the wavelength of the most dangerous mode as a function of the shear stress excess close to the onset of grain motion (see Fig. 4). One sees that the dimensionless wavelength λ_{max}/d moderately increases with increasing shear stress excess and exhibits a significative sensitivity to the grain diameter.

We should finally note that all the unstable modes have a growth rate with a negative imaginary part, indicating a drift in the direction of the flow. The drift velocity of a mode k is easily calculated by: $v_d = -\mathrm{Im}(\omega)/k$. The expression of the drift velocity of the most dangerous mode is given in Table 1 for moderate and high particle Reynolds number.

5 Discussion and conclusion

5.1 Summary of results

We have presented an analytical model for the instability of a sand bed sheared by a turbulent flow. The turbulent

Table 1. Expressions for the wavelength and the drift velocity of the most dangerous mode at moderate and large particle Reynolds number. Re^*_{p0} is the critical particle Reynolds number at the onset of grain motion: $Re^*_{p0} = d\,(s-1)gd\Theta_{0c}/\nu$.

	$10 < Re^*_p < 10^3$	$Re^*_p > 10^4$
λ_{max}	$\frac{0.1}{\delta}\,\frac{\xi Re^*_p}{1+0.087(\xi\,Re^*_p)^{0.75}}\,s\,d$	$\frac{10}{\delta}\,s\,d$
v_d	$60.\,(A\,\delta\,n\,c)\,\sqrt{(s-1)\,\rho_f g d}$ $\times\,\frac{(Re^{*2}_p - Re^{*2}_{p0})^{n-1}}{Re^{*2n}_{p0}}(Re^*_p/\xi)[1+0.087(\xi Re^*_p)^{0.75}]$	$60.\,(A\,\delta\,n\,c)\,\sqrt{(s-1)\,\rho_f g d}$ $\times\,\frac{(Re^{*2}_p - Re^{*2}_{p0})^{n-1}}{Re^{*2n}_{p0}}(Re^*_p/\xi)$

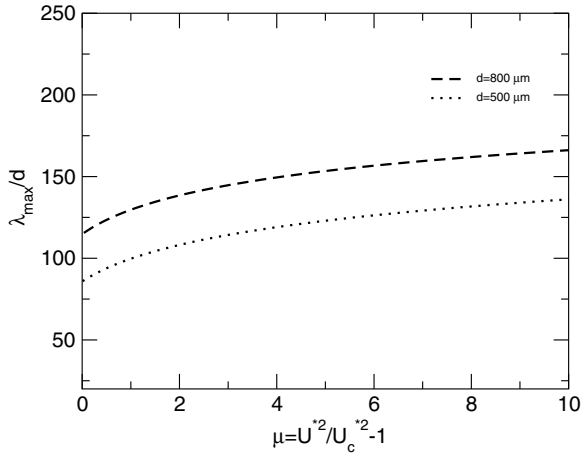

Fig. 4. Wavelength of the most dangerous mode versus the excess shear stress μ for different grain diameters. Parameters: $\theta_{0c} = 0.2$, $s = 2.7$, $\xi = 5$ and $\nu = 10^{-6}\,\mathrm{m}^2/\mathrm{s}$.

flow profile over a perturbed surface is derived on the basis of Jackson and Hunt calculation. The sand transport is assumed to be ensured by a single transport mode which consists of a layer of grains rolling on the surface of the sand bed. The evolution of the bed profile is thus deduced from mass conservation of the grains. The main outcomes of the model follow.

(i) We found a single mode of instability corresponding to the formation of ripple. This instability results from the competition between the destabilizing mechanism due to fluid flow (resulting from the phase lag between the bed shear stress and the bed profile) and a stabilizing effect which originates from the inertia of the grains (characterized by a characteristic length l_{eq} corresponding to the distance needed for a grain at rest to reach its equilibrium velocity). The gravity effect which is usually evoked as the pertinent stabilizing mechanism is found to be inefficient here. The wavelength of the most dangerous mode is found to scale as the equilibrium length l_{eq} which is given by $l_{eq} = f(\xi Re^*_p)\,(\rho_g/\rho_f)\,d$ where f is a function of the particle Reynolds number $Re^*_p = d\,U^*/\nu$ and ξ represents the ratio between the equilibrium velocity U_{eq} of the rolling grains and the shear velocity U^*.

Our results differ from those of Richards model [6]. He found using a rotational flow model based on an eddy viscosity approach and coupled with the Peter-Meyer law for the sediment transport that the most dangerous mode varies linearly with the roughness height y_0 of the bed: $\lambda_{max} \sim f(\phi_s)y_0$ where f is a increasing function of the friction angle ϕ_s of the sand. In our model, the roughness height plays a minor role since it appears in the prefactor of the wavelength of the most dangerous mode via a logarithmic dependence. Furthermore, in Richards model the dominant stabilizing mechanism is due to gravity. If the gravity effect is neglected, modes of arbitrary small wavelength are unstable. This contrasts again with our model where the pertinent stabilizing mechanism originates from the dynamics of the moving grains. Gravity is not found to be efficient to stabilize the modes of short wavelengths (it scales as k^2, in the same manner as the destabilizing process driven by the fluid, but with a much smaller prefactor; see Eq. (22)). As a conclusion, the outcomes of the turbulent flow models appears to be very sensitive to the way of modeling the turbulence. It seems therefore crucial to make additional effort to better describe the turbulent flows over a wavy surface.

5.2 Comparison with available experimental data

As noted by Coleman et al. [9], although the huge number of sand ripple experiments in water reported in the literature, only a few of them can be used for a comparison with stability theory predictions. Indeed, most of the experimental data concern the equilibrium ripple pattern which is reached at long times after a nonlinear transient. The latter is markedly different from the initial pattern observed at the first stages of its development. The wavelength of the final bedform is usually much greater than that of the initial ripple pattern.

Coleman et al collected in [9] some experimental results which can be used for the verification of the theoretical predictions based on linear stability analysis. The conclusion drawn from these experimental data follow. First, it seems that there is a slight increase of the initial ripple wavelength λ with the applied shear stress (within the range of shear stress investigated, which corresponds to values of the relative shear stress excess, μ, comprising between 0 and 10). Second, the ratio λ/d appears to be a slightly decreasing function of grain diameter d and fluctuates between 150 and 300 according to experiments. Recent experimental investigation on sand ripples induced by water shear flow confirms the above features [20]. The predictions of our model are partly in agreement with experimental outcomes. At low relative shear stress excess (i.e., small values of μ), our results showed that the ratio λ/d slightly increases with increasing shear stress. In addition, one found that λ/d gets larger with increasing

grain diameter (see Fig. 4). The last feature is not corroborated by the experiments. In contrast, at high relative shear stress excess, we found that the ripple wavelength is independent of the shear stress and varies linearly with the grain diameter: $\lambda \approx 300\, d$ [see Eq. (27)].

The agreement between experimental results and theoretical predictions is not fully satisfactory and further efforts in theoretical modeling, as well as in experimental investigation, should be done. In particular, it would be strongly needed to investigate in details, both theoretically and experimentally, the erosion and deposition processes at the grain scale in order to improve our understanding of the sediment transport.

5.3 Conclusion

We presented an analytical study about the ripple formation process under turbulent liquid flows in the case of hydraulically rough beds. We proposed a model where the flow over a deformed sand bed is calculated explicitly and the sand transport law accounts for the grain inertia. We derived analytical expressions for the most unstable mode (which is expected to give the order of magnitude of the ripple wavelength), growth rate and drift velocity. The prediction of the model agrees only partially with the available experimental data. There is therefore a strong need to improve the modeling. Several aspects of the sand transport process should be further investigated in the near future. (i) In our model, we do not calculate explicitly the modification of the flow profile due to the presence of the grains in the fluid. It would be therefore important to explicitly take into account the coupling between the transported grains and the flow in order to have an accurate estimation of the equilibrium velocity of the moving grains. (ii) A further effort should be made in the modeling of the erosion and deposition processes at the grain level. This effort is is crucial to improve the description of the sand transport dynamics. (iii) Another important issue concerns the nonlinear process which leads to the final equilibrium ripple pattern. It would be interesting to develop a nonlinear analysis in order to understand the mechanisms of the coarsening process.

I am grateful to C. Misbah for fruitful and enlightening discussions.

Appendix A: Calculation of the turbulent flow over a deformed sand bed

To calculate the flow over a deformed sand bed, the standard strategy is to divide the boundary layer into an inviscid outer region and a thin inner region where the perturbation shear stresses affect the flow (see Fig. 5). The physical reason for this is the following. In the region close to the surface of the perturbed sand bed (the inner region), the horizontal velocity U is given to first order approximation by the velocity above a flat sand bed taken

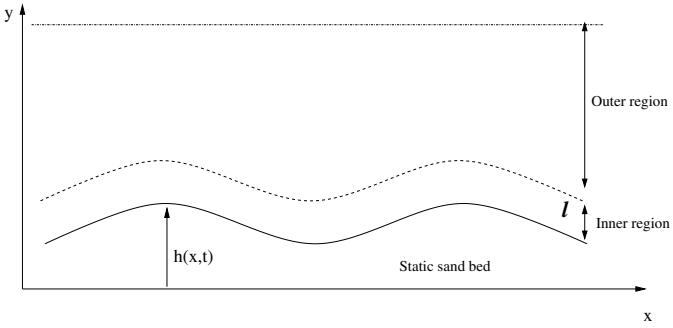

Fig. 5. Schematic diagram of flow regions over a deformed sand bed.

at the same the height with respect to ground level. Thus $U(x,y) = U_0(Y)$ where $Y = y - h(x)$. Continuity implies the existence of a vertical velocity $V = h_x\, U_0(Y)$. But sufficiently far above the bed the horizontal velocity must equal the undisturbed velocity $U_0(y)$ and the vertical velocity must be zero. This suggests therefore the existence of an outer region of flow where $U = U_0(y) + U_1(x,y)$ (the perturbation U_1 must vanish as $y \to \infty$). But in this outer region the perturbation velocity will induce a perturbation pressure P_1. Then the fact that P_1 must be continuous means that there exists a perturbation pressure gradient in the inner region. Thus the horizontal velocity in the inner region can not simply be equal to the displaced velocity $U_0(Y)$ but has a perturbation $U_1(x,Y)$, so that $U = U_0(Y) + U_1(x,Y)$.

A.1 Inner region

In the inner region, as explained previously, we express the perturbed quantities in terms of the displaced coordinates (x,Y) where $Y = y - h(x)$. The perturbed quantities will be written as:

$$U(x,y) = U_0(Y) + U_1(x,Y)\,, \tag{28}$$

$$P(x,y) = P_0 + P_1(x,Y)\,. \tag{29}$$

The subscript 0 refers to the basic solution corresponding to a flat sand bed and the subscript 1 denotes perturbed quantities. From the continuity equation, one can express the vertical component of velocity as

$$V(x,Y) = h_x\,[U_0(Y) + U_1(x,Y)] + V_1(x,Y)\,, \tag{30}$$

where

$$\frac{\partial U_1}{\partial x} + \frac{\partial V_1}{\partial Y} = 0\,. \tag{31}$$

In the further analysis, we will require that $h_x \sim h_1 k$ is a small quantity which is at least of the same order as the perturbed velocity U_1/U^*. This will be checked a posteriori.

The component of the perturbed Reynolds stress tensor reads

$$\tau_{xy} = \rho_f \kappa^2 Y^2 \left(\frac{\partial U}{\partial y}\right)^2 = \sigma_0 + \sigma_1 + h.o.t.\,, \tag{32}$$

$$\tau_{yy} = 2\rho_f \kappa^2 Y^2 \left(\frac{\partial U}{\partial y}\right)\left(\frac{\partial V}{\partial y}\right) = \varsigma_1 + h.o.t.\,, \tag{33}$$

where

$$\sigma_0 = \rho_f U^{*2}\,, \tag{34}$$

$$\sigma_1 = 2\rho_f\,\kappa\,U^* Y \frac{\partial U_1}{\partial Y}\,, \tag{35}$$

$$\varsigma_1 = 2\rho_f\,\kappa\,U^* Y \frac{\partial V_1}{\partial Y}\,. \tag{36}$$

We recall that $\tau_{xx} = 0$ because the horizontal turbulent viscosity is neglected.

Plugging equations (28),(29), (30), (32 and (33) into the momentum and mass conservation equations for the flow and retaining only the first order terms, we obtain:

$$U_0\frac{\partial U_1}{\partial x} + V_1\frac{\partial U_0}{\partial Y} = -\frac{1}{\rho_f}\frac{\partial P_1}{\partial x} + \frac{1}{\rho_f}\frac{\partial \sigma_1}{\partial Y}\,, \tag{37}$$

$$U_0\frac{\partial V_1}{\partial x} = -\frac{1}{\rho_f}\frac{\partial P_1}{\partial Y} + \frac{1}{\rho_f}\left[\frac{\partial \sigma_1}{\partial x} + \frac{\partial \varsigma_1}{\partial Y}\right]\,, \tag{38}$$

$$\frac{\partial U_1}{\partial x} + \frac{\partial V_1}{\partial Y} = 0\,. \tag{39}$$

Taking the Fourier transform with respect to the variable x, we can rewrite the above equations as

$$ik\ln\left(\frac{Y}{y_0}\right)\hat{U}_1 + \frac{\hat{V}_1}{Y} = -\kappa(ik)\hat{P}_1 + 2\kappa^2\left(Y\frac{\partial \hat{U}_1}{\partial Y}\right)\,, \tag{40}$$

$$ik\ln\left(\frac{Y}{y_0}\right)\hat{V}_1 = - \kappa\frac{\partial \hat{P}_1}{\partial Y} + 2\kappa^2\left[ikY\frac{\partial \hat{U}_1}{\partial Y} + \frac{\partial}{\partial Y}\left(Y\frac{\partial \hat{V}_1}{\partial Y}\right)\right]\,, \tag{41}$$

$$ik\hat{U}_1 + \frac{\partial \hat{V}_1}{\partial Y} = 0\,, \tag{42}$$

where $\hat{U}_1 = TF(U_1/U^*)$, $\hat{V}_1 = TF(V_1/U^*)$, and $\hat{P}_1 = TF(P_1/\rho_f U^{*2})$. TF stands for the Fourier transform.

We shall introduce a stretched variable $Z = Y/l$, where we recall that l is the width of inner region. We can rewrite the equations of the flow in terms of the stretched variable. We get:

$$ikl\left(\ln\frac{l}{y_0} + \ln Z\right)\hat{U}_1 + \frac{\hat{V}_1}{Z} = -\kappa(ikl)\hat{P}_1 + 2\kappa^2\frac{\partial}{\partial Z}\left(Z\frac{\partial \hat{U}_1}{\partial Z}\right)\,, \tag{43}$$

$$ikl\left(\ln\frac{l}{y_0} + \ln Z\right)\hat{V}_1 = -\kappa\frac{\partial \hat{P}_1}{\partial Z} + 2\kappa^2\left[i(kl)\,Z\frac{\partial \hat{U}_1}{\partial Z} + \frac{\partial}{\partial Z}\left(Z\frac{\partial \hat{V}_1}{\partial Z}\right)\right]\,, \tag{44}$$

$$i(kl)\,\hat{U}_1 + \frac{\partial \hat{V}_1}{\partial Z} = 0\,. \tag{45}$$

The inner region is defined as the layer where the Reynolds stress tensor term competes with the inertial term. The width of the inner region will be therefore determined by the balance between these two terms at $Y = l$ (or $Z = 1$). This gives

$$kl\ln\frac{l}{y_0}\hat{U}_1 \simeq 2\kappa^2\hat{U}_1. \tag{46}$$

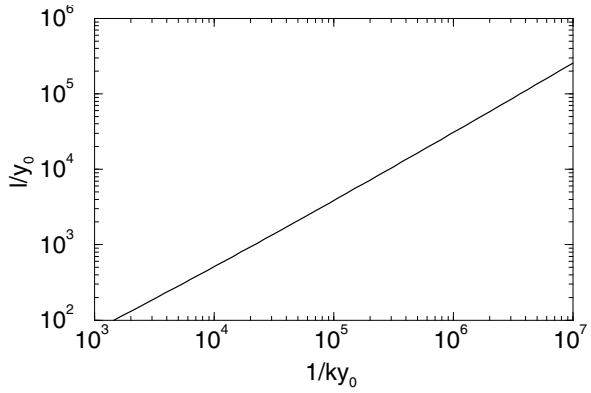

Fig. 6. Depth of the inner region l as a function of $1/ky_0$.

As a consequence we will define l such that $kl\ln(l/y_0) = 2\kappa^2$. The graph of l/y_0 as a function of $1/ky_0$ is shown in Figure 6. To go further, we will introduce a small parameter $\delta = 1/\ln(l/y_0) = kl/2\kappa^2$. δ is small as long as the wavelength of the perturbation is much greater than l. This means that we examine the long wavelength limit. More precisely, the range of values of ky_0 for which δ is small (let say $\delta < 0.2$) is found to be such that $10^{-6} < ky_0 < 10^{-2}$. Over this range, the width of the inner region can be expressed within 5% by the following approximate expression:

$$\frac{l}{y_0} = a\left(\frac{1}{ky_0}\right)^b\,, \tag{47}$$

with $a = 0.21$ and $b = 0.85$. Using this formula, we can derive an approximate expression for δ

$$\delta = \frac{a}{2\kappa^2}(ky_0)^{1-b} \simeq 0.65\,(ky_0)^{0.15}\,. \tag{48}$$

The strategy is now to expand $\hat{U}_1$, $\hat{V}_1$ and $\hat{P}_1$ in power of δ:

$$\hat{U}_1 = \varepsilon(\hat{U}^{(0)} + \delta\hat{U}^{(1)} + \dots)\,, \tag{49}$$

$$\hat{V}_1 = \varepsilon(\delta\hat{V}^{(0)} + \delta^2\hat{V}^{(1)} + \dots)\,, \tag{50}$$

$$\hat{P}_1 = \frac{\varepsilon}{\delta}(\hat{P}^{(0)} + \delta\hat{P}^{(1)} + \dots)\,. \tag{51}$$

ε is a small parameter which is introduced to provide a scale for the perturbation velocities and will be determined later on. One should note that the perturbation velocity $\hat{U}_1$ scales as ε whereas the pressure perturbation is expected to scale as ε/δ. This is due to the fact that the pressure gradient must be of the same order as the acceleration and the stress gradient term in equation (43) since the velocity perturbation is driven by the pressure perturbation. To zero and first order, equations (43–45)

yield

$$\frac{\partial}{\partial Z}\left(Z\frac{\partial}{\partial Z}\hat{U}^{(0)}\right) - iU^{(0)} = i\kappa\hat{P}^{(0)}\,, \tag{52}$$

$$\frac{\partial\hat{P}^{(0)}}{\partial Y} = 0\,, \tag{53}$$

$$i2\kappa^2U^{(0)} + \frac{\partial V^{(0)}}{\partial Z} = 0\,, \tag{54}$$

$$\frac{\partial}{\partial Z}\left(Z\frac{\partial}{\partial Z}\hat{U}^{(1)}\right) - i\hat{U}^{(1)} = i\kappa\hat{P}^{(1)} + i\ln Z\hat{U}^{(0)} + \frac{\hat{V}^{(0)}}{2\kappa^2 Z}\,, \tag{55}$$

$$\frac{\partial\hat{P}^{(1)}}{\partial Y} = 0\,, \tag{56}$$

$$i2\kappa^2U^{(0)} + \frac{\partial V^{(0)}}{\partial Z} = 0\,, \tag{57}$$

which should be completed by the boundary conditions. As $Z \to 0$, the solution should match the velocity profile very close to the surface which is assumed to be logarithmic:

$$U = \frac{\sqrt{\sigma/\rho_f}}{\kappa}\ln(\frac{Y}{y_0})\,, \tag{58}$$

where $\sigma = \sigma_0 + \sigma_1$ is the total bed shear stress. Expanding σ_1 in power of δ [i.e., $\sigma_1 = \varepsilon(\delta\sigma^{(0)} + \delta^2\sigma^{(1)})$] and plugging this expansion into equation (58), we find that the perturbed velocity $\hat{U}_1$ should obey the following boundary conditions as $Z \to 0$:

$$\hat{U}^{(0)} \sim \frac{\hat{\sigma}^{(0)}}{2\kappa}\,, \tag{59}$$

$$U^{(1)} \sim \frac{\hat{\sigma}^{(0)}}{2\kappa}\ln Z + \frac{\hat{\sigma}^{(1)}}{2\kappa}\,. \tag{60}$$

The general solution of the equation for $\hat{U}^{(0)}$ [Eq. (52)] is of the form:

$$\hat{U}^{(0)} = A\,K_0(2\sqrt{iZ}) + B\,I_0(2\sqrt{iZ}) - \kappa P^{(0)} \tag{61}$$

K_0 and I_0 are the modified Bessel functions whereas A and B are integration constants to be determined by use of the boundary conditions which expressed in terms of the stretched variable read:

$$\hat{U}^{(0)}(Z \to \infty) < \infty\,, \tag{62}$$

$$\hat{U}^{(0)}(Z \to 0) = \frac{\hat{\sigma}^{(0)}}{2\kappa}\,. \tag{63}$$

Taking advantage of the boundary conditions, we obtain $A = B = 0$ and $\hat{\sigma}^{(0)} = -2\kappa^2\hat{P}^{(0)}$. From continuity eq. (54), we obtain:

$$V^{(0)} = 2i\kappa^3P^{(0)}Z\,. \tag{64}$$

One should go to next order to get a non-trivial solution for U. The solution of the equation for $U^{(1)}$ [Eq. (55)] reads

$$\hat{U}^{(1)} = C\,K_0(2\sqrt{iZ}) + D\,I_0(2\sqrt{iZ}) - \kappa\hat{P}^{(0)}\left[1 - \ln Z\right]\,. \tag{65}$$

C and D are integration constants to be determined by use of the boundary conditions:

$$\hat{U}^{(1)}(Z \to \infty) < \infty\,, \tag{66}$$

$$\hat{U}^{(1)}(Z \to 0) = \frac{\hat{\sigma}^{(0)}}{2\kappa}\ln Z + \frac{\hat{\sigma}^{(1)}}{2\kappa}\,, \tag{67}$$

which yield:

$$C = -4\kappa\hat{P}^{(0)}\,, \quad D = 0\,, \tag{68}$$

$$\sigma^{(1)} = -2\kappa^2\left(1 + 4\gamma + i\pi\right)\,. \tag{69}$$

$\gamma = 0.57$ is the Euler constant. It should be noted that in the derivation of $\hat{U}^{(1)}$ we assumed that the first order perturbation pressure, $\hat{P}^{(1)}$, is reduced to a zero constant. This approximation allows to shorten the calculations without altering the final result.

The solution $\hat{U}^{(1)}$ can be rewritten as:

$$\hat{U}^{(1)} = -\kappa\hat{P}^{(0)}\left[1 - \ln Z - 4K_0(2\sqrt{iZ})\right]\,. \tag{70}$$

Using expressions of $\hat{\sigma}^{(0)}$ and $\hat{\sigma}^{(1)}$, one can estimate the perturbed bed shear stress σ_1 which reads:

$$\hat{\sigma}_1 = -2\varepsilon\kappa^2\delta\hat{P}^{(0)}\left[1 + \delta(1 + 4\gamma + i\pi)\right]\,. \tag{71}$$

The pressure $\hat{P}^{(0)}$ will be deduced from the examination of the flow in the outer region.

A.2 Outer region

In the outer region, we express the perturbed quantities in terms of the original coordinates (x, y). Therefore the perturbed quantities will be written as:

$$U = U_0(y) + U_1(x, y)\,, \tag{72}$$

$$V = V_1(x, y)\,, \tag{73}$$

$$P = P_0 + P_1(x, y)\,. \tag{74}$$

In the outer region the Reynolds stress is negligible in comparison with the inertial terms so that the equations of the flow read to first order:

$$ik\ln\left(\frac{y}{y_0}\right)\hat{U}_1 + \frac{\hat{V}_1}{y} = -\kappa(ik)\hat{P}_1\,, \tag{75}$$

$$ik\ln\left(\frac{y}{y_0}\right)\hat{V}_1 = -\kappa\frac{\partial\hat{P}_1}{\partial y}\,, \tag{76}$$

$$ik\hat{U}_1 + \frac{\partial\hat{V}_1}{\partial y} = 0\,. \tag{77}$$

We recall that $\hat{U}_1 = TF(U_1/U^*)$, $\hat{V}_1 = TF(V_1/U^*)$ and $\hat{P}_1 = TF(P_1/\rho_f U^{*2})$.

The vertical length scale in the outer region is expected to be of order of $1/k$ and it is therefore natural to rewrite $\ln(y/y_0)$ as:

$$\ln(y/y_0) = \ln(1/ky_0) + \ln(yk)\,. \tag{78}$$

As $y \sim 1/k$, the later expression can seen as an asymptotic development as a function of the small parameter $\ln^{-1}(1/ky_0)$. We therefore expand $\hat{U}_1$, $\hat{V}_1$ and $\hat{P}_1$ in power of $\delta_1 = \ln^{-1}(1/ky_0)$:

$$\hat{U}_1 = \frac{\varepsilon}{\delta}\left(\delta_1\hat{u}^{(0)} + \delta_1^2\hat{u}^{(1)} + \dots\right)\,, \tag{79}$$

$$\hat{V}_1 = \frac{\varepsilon}{\delta}\left(\delta_1\hat{v}^{(0)} + \delta_1^2\hat{v}^{(1)} + \dots\right)\,, \tag{80}$$

$$\hat{P}_1 = \frac{\varepsilon}{\delta}\left(\hat{p}^{(0)} + \delta_1\hat{p}^{(1)} + \dots\right)\,. \tag{81}$$

The perturbation pressure has been taken to scale as ε/δ since it has the same order of magnitude in the outer region as in the inner region. To leading order, equations (75-77) yields:

$$\hat{u}^{(0)} = -\kappa\hat{p}^{(0)}\,, \tag{82}$$

$$ik\hat{v}^{(0)} = -\kappa\frac{\partial\hat{p}^{(0)}}{\partial y}\,, \tag{83}$$

$$ik\hat{u}^{(0)} = -\frac{\partial\hat{v}^{(0)}}{\partial y}\,. \tag{84}$$

Combining these equations, we get a closed equation for $\hat{v}^{(0)}$:

$$\frac{\partial^2\hat{v}^{(0)}}{\partial y^2} - \hat{v}^{(0)} = 0\,, \tag{85}$$

which is subject to the following boundary conditions:

$$\hat{v}^{(0)}(y\to\infty) < \infty\,, \tag{86}$$

$$\hat{v}^{(0)}(yk\to 0) = ikh_1\frac{\delta}{\kappa\delta_1^2\varepsilon}\,. \tag{87}$$

The last condition results from the matching of the inner and outer solution of the vertical velocity. Since by definition $v^{(0)}$ is $O(1)$, we deduce the magnitude of ε:

$$\varepsilon = \frac{\delta}{\kappa\delta_1^2}h_1 k\,. \tag{88}$$

Taking advantages of the boundary conditions, we find:

$$\hat{v}^{(0)} = ie^{-y|k|}\,. \tag{89}$$

We can therefore deduce the expression for the pressure:

$$\hat{p}^{(0)} = -\frac{|k|}{\kappa k}e^{-|k|y}\,. \tag{90}$$

The pressure at the boundary between the inner and the outer region is then given by $\hat{p}^{(0)}(yk\to 0) = \hat{P}^{(0)} = -|k|/(\kappa k)$. Plugging the expression for the pressure into equation (71), we get the sought after expression of the shear stress at the sand bed:

$$\hat{\sigma}_1 = 2\,A\,h_1\,|k|\,[1 + \delta(1 + 4\gamma + i\pi)]\,, \tag{91}$$

where $A = \delta^2/\delta_1^2$. Expression (91) is a similar form as that found in [18,19] for an isolated perturbation.

References

1. J. Fredsoe, R. Deigaard, *Mechanics of Coastal Sediment Transport* (World Scientific, 1992)
2. J.F. Kennedy, J. Fluid Mech. **16**, 521 (1963)
3. J.F. Kennedy, Ann. Rev. Fluid Mech. **1**, 147 (1969)
4. M.H. Gradowczyk, J. Fluid Mech. **33**, 93 (1968)
5. S.E. Coleman, J.D. Fenton, J. Fluid Mech. **418**, 101 (2000)
6. K.J. Richards, J. Fluid Mech. **99**, 597 (1980)
7. B.M. Sumer, M. Bakioglu, J. Fluid Mech. **144**, 117 (1984)
8. J.D. Smith, S.R. McLean, J. Geophys. Res. **82**, 1735 (1977)
9. S.E. Coleman, B.W. Melville, J. Hydr. Engng. ASCE **122**, 301 (1996)
10. A.J. Raudkivi, J. Hydr. Engng. **123**, 58 (1997)
11. F. Charru, H. Mouilleron-Arnould, J. Fluid Mech. **452**, 303 (2002)
12. A. Valance, V. Langlois, Eur. Phys. J. B **43**, 283 (2005)
13. P.S. Jackson, J.C.R. Hunt, Quart. J. R. Met. Soc. **101**, 929 (1975)
14. L. Prandtl, *The mechanics of viscous fluid*, edited by W.F. Durand, Vol. III (1935)
15. J. Nikuradse, V.D.I.-Forschungheft **361** (1933)
16. G. Sauermann, K. Kroy, H.J. Herrmann, Phys. Rev. E **64**, 0321305 (2001)
17. B. Andreotti, P. Claudin, S. Douady, Eur. Phys. J. B **28**, 315 (2002)
18. J.C.R. Hunt, S. Leibovich, K.J. Richards, Quart. J. R. Met. Soc. **114**, 1435 (1988)
19. W.S Weng, J.C.R. Hunt, D.J. Carruthers, A. Warren, G.F.S. Wiggs, I Livingstone, I. Castro, Acta Mechanica Suppl. **2**, 1–22 (1991)
20. A. Betat, V. Frette, I. Rehberg, Phys. Rev. Lett. **83**, 88 (1999)